A peri-Gondwanan arc in NW Iberia. II: Assessment of the intra-arc tectonothermal evolution through U–Pb SHRIMP dating of mafic dykes

F. Díaz García [a], S. Sánchez Martínez [b], P. Castiñeiras [c], J.M. Fuenlabrada [d], R. Arenas [c,*]

[a] Departamento de Geología, Universidad de Oviedo, 33005 Oviedo, Spain
[b] Institut für Geowissenschaften, Mineralogie–Petrologie und Geochemie, Goethe-Universität, Altenhöferallee 1, D-60438 Frankfurt am Main, Germany
[c] Departamento de Petrología y Geoquímica e Instituto de Geología Económica (CSIC), Universidad Complutense de Madrid, 28040 Madrid, Spain
[d] CAI de Geocronología y Geoquímica Isotópica, Facultad de Geología, Universidad Complutense de Madrid, 28040 Madrid, Spain

Keywords:
Arc dynamics
Cambrian intra-arc deformation
U–Pb SHRIMP dating
Peri-Gondwanan arc
Allochthonous complexes
NW Iberia

A B S T R A C T

The arc-derived upper units of the Órdenes Complex, NW Iberia, are emplaced above the Variscan suture and contain a low-grade metasedimentary uppermost section, with a maximum depositional age of 510–530 Ma, intruded by a number of mafic dykes. Three deformational events affect the metasedimentary section. The youngest deformation event (D_3) is of undifferentiated Variscan age and consists of metre- to decametre-scale, close upright folds with axes plunging gently towards N20°E. The most important D_2 structure is a regional S_2 foliation axial planar of minor folds with dextral asymmetry. The presence of a stretching lineation parallel to the D_2 fold axes is related to a top-to-the-north sense of shearing in a context of regional extension. The oldest meter-scale D_1 folds are developed in suitable greywacke–pelite alternations and consist of tight folds with chevron and similar morphologies, axes plunging gently toward N20°E, and a continuous S_1 axial planar foliation. The essential characteristic of the D_1 deformation event is depicted by a set of west-vergent folds with reverse limbs less than 2 km in wavelength, that are affected

The age of D_2 and D_1 structures is not well constrained. The diabase dykes intruding the low-grade turbidites cut the D_1 folds and their field relationships suggest that they were emplaced at the end of the D_2 shearing event and prior to the upright D_3 Variscan folds. Zircon grains obtained from one of the diabase dykes were analysed for U–Pb at the SHRIMP-RG facility at Stanford University. An age of c. 510 Ma, based on the analysis of 31 individual zircon grains, is interpreted to date the crystallization of the Ares dyke. The tectonic and magmatic evolution of the top turbiditic series of the Órdenes Complex is tentatively related to the dynamics of a peri-Gondwanan arc developed during active subduction beneath Gondwana and suggests: (1) accretion beneath the arc during west-vergent (present coordinates) nappe development (D_1); (2) extension of the arc during top-to-the-north shearing (D_2); and (3) final intrusion of the diabasic dykes into an intra-arc turbiditic series. This evolution spans the end of volcanic arc activity and the onset of the opening of the Rheic Ocean.

1. Introduction

The arc-derived upper units of the allochthonous complexes of NW Iberia include a thick turbiditic series that occupies the uppermost structural position. An earlier first companion paper in this issue (Fuenlabrada et al., 2010) describes the geochemistry of the turbidites and their provenance based on new Nd isotope data and a revision of previously published U–Pb ages for detrital zircon grains (Fernández-Suárez et al., 2003). Fuenlabrada et al. (2010) also provide a general description of the tectonothermal evolution of the upper units based on field evidence and U–Pb ages (Abati et al., 1999, 2007; Fernández-Suarez et al., 2002, 2007; Ordoñez Casado et al., 2001). Present data suggest an intra-arc setting for the sedimentary basin in which the turbiditic series was deposited, located in a peri-Gondwanan realm peripheral to the margin of the West African Craton. The volcanic arc was probably built on the most external margin of Gondwana on thinned continental basement. The Nd isotopic data suggest an affinity with West Avalonia, Florida and the Carolina terrane, and a more westerly provenance than that accepted for the Early Paleozoic autochthonous sequence in NW Iberia and its equivalents in the Bohemian Massif (Linnemann and Romer, 2002), largely confirming earlier data on the provenance of this allochthonous terrane (Gómez Barreiro et al., 2007).

This paper presents a detailed structural and microstructural analysis of the turbiditic series from the coastal section of the Ares–Sada region, east of A Coruña city (Fig. 1), and U–Pb age data for diabase dykes intruding the sedimentary succession. Structural analysis of the low-grade uppermost section of the upper units complements the history recorded in the rest of the upper units for two reasons. First, minor recrystallization and grain growth favour the preservation of old

* Corresponding author. Departamento de Petrología y Geoquímica, Facultad de Geología, Universidad Complutense de Madrid, C/ José Antonio Novais, no 2, 28040 Madrid, Spain.
E-mail address: arenas@geo.ucm.es (R. Arenas).

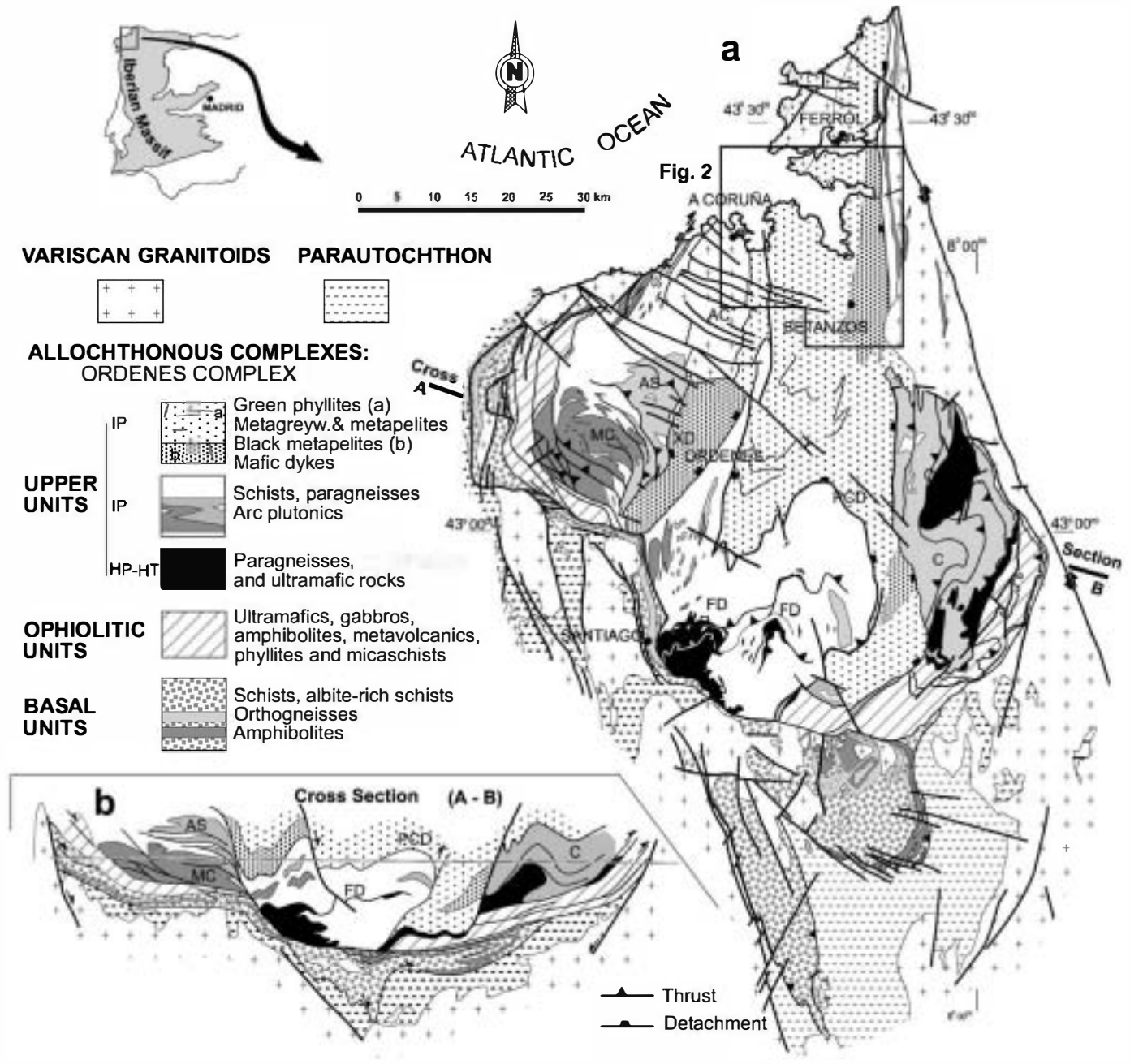

Fig. 1. (a) Structural map, and (b) cross section of the Órdenes Complex showing location of area depicted in Fig. 2. AC, A Coruña granodiorite; AS, A Silva granodiorite; C, Corredoiras granodiorite; CD, Corredoiras detachment; F, Fornás unit; FD, Fornás detachment; MC, Monte Castelo gabbro; PCD, Ponte Carreira detachment; S, Sobrado unit; XD, Xesteda detachment.

structures, such that the unit provides unique information about early stages in the tectonic evolution of the upper units which is usually lost elsewhere as a result of higher grade metamorphic recrystallization. Second, large numbers of mafic dykes intrude the low-grade metasediments and show various relationships with the regional deformation events. The relative timing of mafic dyke emplacement can be established by field relationships, and the new U–Pb age of dyke emplacement can be used to date the structural evolution of this uppermost section. The age data and cross-cutting relationships clearly indicate that this part of the upper units was deformed in Middle Cambrian times. This structural evolution therefore provides important information about the dynamics of the peri-Gondwanan arc represented in the upper allochthonous terrane of NW Iberia, including the structures and kinematics developed during the transition between the contractional and extensional regimes that preceded the Cambro-Ordovician opening of the Rheic Ocean at the periphery of the West African Craton.

2. Structure of the upper units at the Ares–Sada region: the coastal section

In contrast to the rest of the upper units, which are characterized by a pervasive regional S_2 foliation developed under medium- to high-grade conditions that prevents analysis of earlier deformation events, their uppermost low-grade unit can be studied as a typical slate belt by applying classical macroscopic and microscopic geometrical analysis and superpositional criteria. On this basis, three main deformation events can be distinguished, each associated with different structures and kinematics. Hence, the uppermost unit provides a unique opportunity to identify the earliest deformation event in the upper units of the

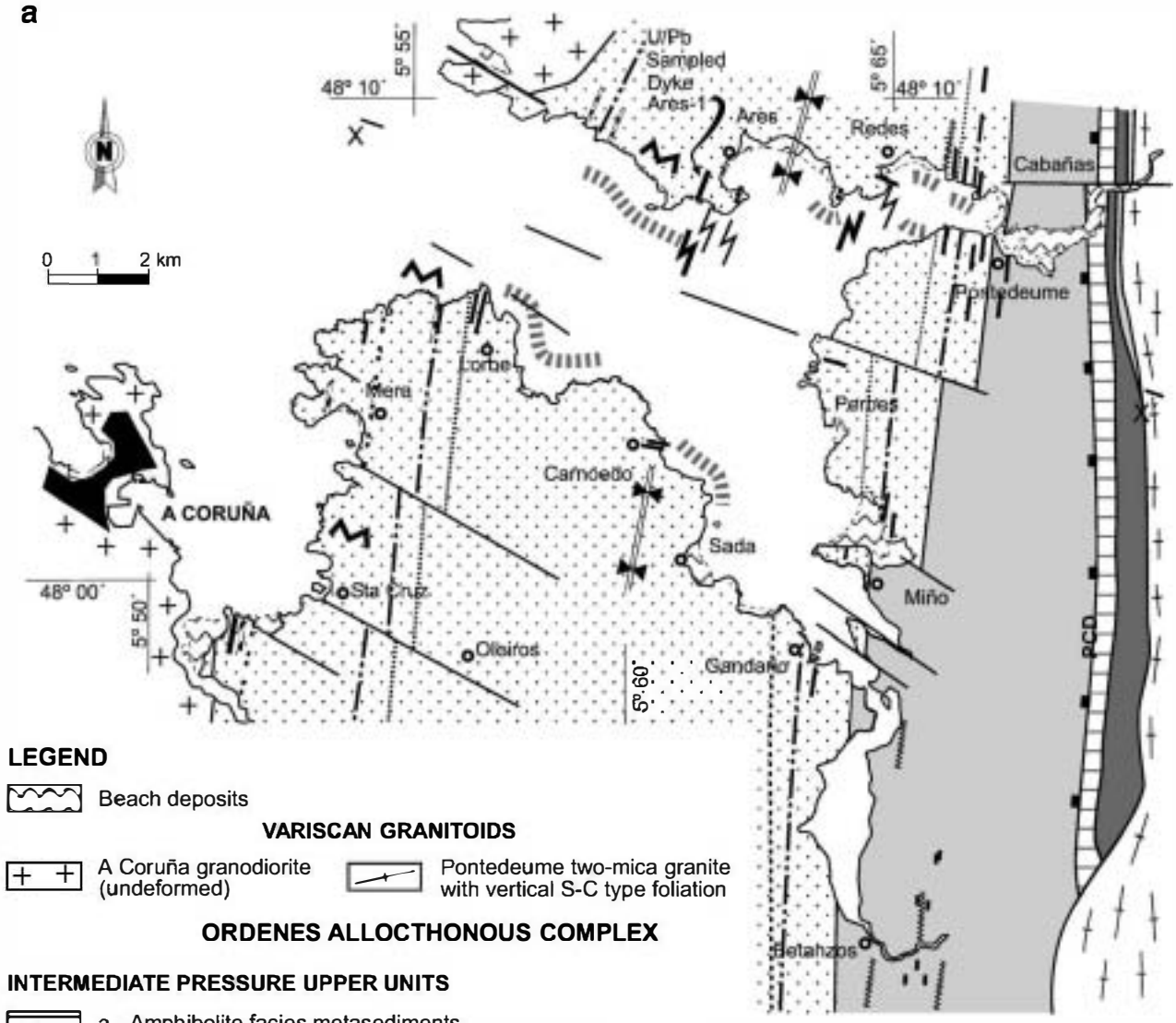
a
U/Pb Sampled Dyke Ares-1
48° 10'
5° 55'
5° 65'
Ares
Redes
Cabañas
Pontedeume
Lorbe
Mera
Perbes
Carnoedo
Sada
A CORUÑA
48° 00'
5° 50'
Sta Cruz
Oleiros
Miño
PCD
5° 60'
Gandaro
Betanzos
0 1 2 km
N
LEGEND
Beach deposits
VARISCAN GRANITOIDS
A Coruña granodiorite (undeformed)
Pontedeume two-mica granite with vertical S-C type foliation
ORDENES ALLOCTHONOUS COMPLEX
INTERMEDIATE PRESSURE UPPER UNITS
a - Amphibolite facies metasediments
b - Gabbros
c - Granodioritic gneiss
Uppermost turbiditic formation
Metagreywacke and metapelite alternancies
a - Conglomeratic levels
b - Calc-silicate layers
Black metapelites (lower part)
a - Black quartzites
Diabase dyke undeformed and folded
Ponte Carreira Detachment (PCD)
D2 Deformation front
Sectors with reverse stratigraphic polarity
Minor fold asymmetry F1
Minor fold asymmetry F3
Biotite in
Garnet in

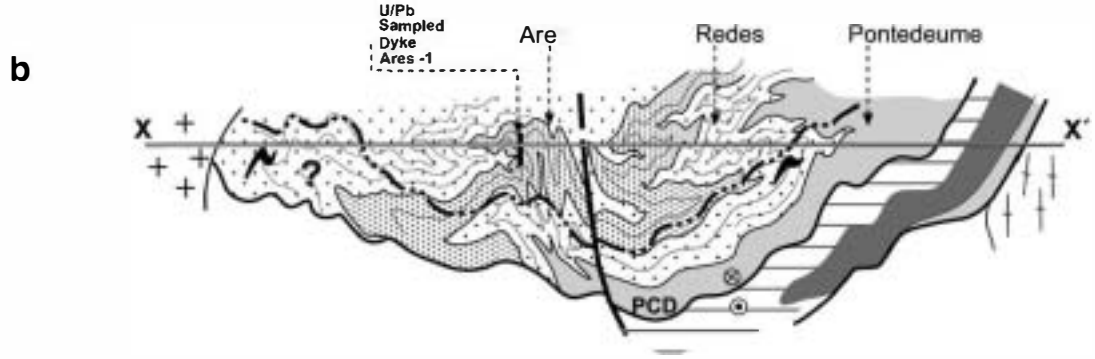
b
U/Pb Sampled Dyke Ares -1
Are
Redes
Pontedeume
X
X'
PCD

allochthonous complexes. The three deformation events are described below, starting with the most recent.

The youngest deformation event (D_3) consists of metre- to decametre-scale folding developed throughout the entire unit and comprising close, upright structures with axes plunging gently N20°E. Centimetre-wide greywacke layers show flattened parallel folds, sometimes developing cuspate–lobate forms. A near-vertical axial planar crenulation cleavage (S_3) is always present and is better developed in metapelitic beds. These beds sometimes show strong differentiation with a spaced, non-penetrative crenulation cleavage that is less evident, discontinuous or absent, in the metagreywackes. In the coastal section (Figs. 1 and 2) meter-scale D_3 folds show opposite asymmetry, defining a major D_3 synform, the enveloping surface of which is shown in cross-section in Fig. 2b and can be followed inland, where it defines the major Órdenes synform (Fig. 1). This major synform belongs to a widespread Variscan refolding phase in the Órdenes Complex that affected the stacking of allochthonous units and their bounding shear zones (e.g., (Martínez Catalán et al., 1996)).

Structures belonging to the older D_2 deformational event affect almost all the upper units, but in the study area an upper deformation front can be traced parallel to the "biotite in" boundary (Fig. 2). The most important structure of this event is a regional S_2 foliation that shows various microstructures corresponding to early and intermediate stages in the morphological evolution of a crenulation cleavage under increasing deformation and temperature, as proposed by Passchier and Trouw (2005). Although strongly affected by upright folding, it is assumed that S_2 was initially subhorizontal. The foliation is axial planar of minor folds that are dextral in asymmetry, and sometimes non-cylindrical with the intensely sheared short limbs. This feature, together with the presence of a stretching lineation parallel to the fold axes, suggests top-to-the-north sense of shear. At deeper structural levels the S_2 foliation is a highly evolved compositional foliation, the development of which was coeval with amphibolite facies metamorphism (Castiñeiras, 2005). Towards the base of the intermediate pressure upper units, partial melting of the metasediments took place during the final stages of S_2 development, which shows a metatexitic appearance and is locally disaggregated by diatexite. U–Pb analysis of monazites from metatexites has yielded an age of 490 Ma (Abati et al., 1999). This apparently structural continuity is interrupted by the development of a major extensional shear zone, the Ponte Carreira detachment (Martínez Catalánet al., 2002; Gomez Barreiro, 2007) (PCD in Fig. 2), which led to the thinning of the garnet and staurolite zones, strong retrogression and phyllonitization, and the formation of C′ shear bands (Berthé et al., 1979). The mineral stretching lineation parallel to D_2 fold axes is well defined in these rocks where it is aligned north–south and indicates top-to-the-north sense of shear.

The first deformation event (D_1) was probably present throughout the intermediate pressure upper units, although at lower structural levels no major structures have been identified, and D_1 is represented only by an S_1 cleavage strongly overprinted by S_2. In fact, it is only recognizable in relict D_2 fold hinges or as oriented inclusion trails in garnet or staurolite porphyroblasts. The low-grade turbiditic rocks on the coastal section near Ares, however, are devoid of D_2 deformation and so are suitable for the study of minor D_1 fold asymmetries. Combining this with the angular relationships between the existing foliations (S_1 and S_3) and bedding (S_0), and the younging direction of the strata, allows the position of the fold hinges to be located and provides a means of determining fold facing vs. vergence in polyphase folded terrains. Metre-scale folds developed in alternating greywackes and pelites are tight with chevron and similar morphologies. Their axial planes have varying orientations as a consequence of late D_3 folding, but their axes plunge gently towards N20°E. The axial

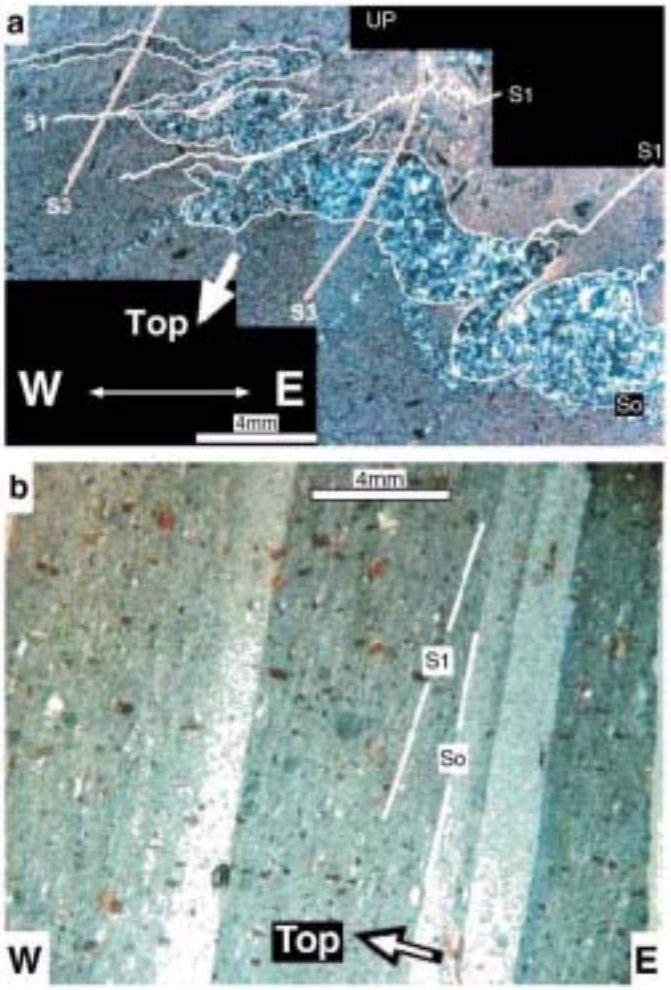

Fig. 3. Microstructural aspects of the different types of foliation in the low-grade part of the upper units and their angular relationships that, together with the presence of graded bedding, suggest a west vergence for the D_1 fold nappe. (a) Minor "Z shaped" folds developed in the reverse limb of a west-vergent D_1 fold that was later affected by a crenulation cleavage (S_3). (b) Angular relationship between bedding (S_0) and slaty cleavage (S_1) within the normal limb of a minor downward facing D_1 fold.

planar S_1 cleavage is a pervasive slaty cleavage at a low angle to the bedding and is well developed in the metapelitic tops of the turbiditic strata. In thin section, S_1 is a continuous foliation (*sensu* (Passchier and Trouw, 2005)) mainly defined by flattened and elongate quartz grains and the non-domainal homogeneous distribution of platy mineral grains with a preferred orientation. The younging direction deduced from graded bedding in greywacke layers shows frequent changes, from which it can be inferred that the largest D_1 reverse limbs never exceed 1 km in wavelength.

Decametre- and centimeter-scale, upward facing D_1 folds can be observed in the western limb of the major Órdenes D3 synform. From these the sinistral asymmetry of a major west-vergent fold can be deduced. In the eastern limb of the Órdenes D_3 synform, suitable minor folds have not been found, but microscopic analysis of oriented samples of S_1, S_3 and S_0 angular relationships suggests a west vergence for this first deformation event (Fig. 3). Thus, the structural and younging criteria discussed above, together with the main stratigraphic features of the area permit the reconstruction of the cross section shown in Fig. 2b. Here, the structural architecture is depicted by a set of west-vergent D_1 folds that have reverse limbs less than 2 km in wavelength and are

Fig. 2. (a) Geological map of the Ares-A Coruña–Betanzos region showing the main lithologies, the sectors with reverse stratigraphic polarity, and the asymmetry of minor folds of the different deformation events. (b) Interpretive cross sections accounting for the presence of several sectors with reverse stratigraphic polarity and S_0/S_1 angular relationships. The structural level with abundant of conglomerates and thick greywacke layers has been highlighted. The location of the dated diabase dyke is also shown.

affected in their lower part by the general presence of the regional S_2 foliation, the development of which culminates in the formation of the Ponte Carreira detachment. The whole package is then overprinted by upright D_3 Variscan folding.

3. Relative timing of dyke emplacement

From a regional point of view, mafic dykes are almost exclusive to the low-grade part of the upper units and are likely linked to the major igneous bodies in the underlying section. Their absence in the remaining part of the orogenic section, however, suggests that they were emplaced prior to the stacking of the allochthonous units. The sills and cross-cutting dykes show a rectilinear geometry and range from 20–30 cm to 20–30 m in thickness, both in map view and in vertical exposures. Individual dyke segments are sub-parallel (from N30°E to N15°W) and perpendicular (N110°E) to the regional foliation (S1 or S2). The dykes are mainly composed of medium-grained gabbro and diabase showing chilled margins, and consist of plagioclase, hornblende, epidote and sphene with minor amounts of quartz and relict pyroxene. The similarity of the macroscopic appearance, phase assemblages, and textures of the gabbroic and diabasic dykes and sills precludes field and petrographic distinction of different magma series. Mafic dykes in the lower part of the study area show clear cross-cutting relationships with the S_2 foliation, but some are boudinaged and sheared at their margins. Syntectonic garnet growth in these sheared margins points to a syn- to post-tectonic intrusion with respect to the regional S_2 foliation. In the uppermost part of the unit, which is devoid of S_2, the mafic dykes are undeformed and transect D_1 folds. Conversely, a number of thin, rectilinear diabase dykes are folded by upright D_3 Variscan folds. In addition, a number of quartz veins were formed at high angles to the S_1 cleavage during D_2. The presence of these veins together with the diabase dyke swarm suggests the existence of a dilational event that may be linked to brittle behaviour during the final stages of D_2.

4. U–Pb dating of the dyke network

4.1. Analytical methods

Zircon crystals from the Ares dyke were separated at Universidad Complutense (Madrid) using conventional gravimetric and magnetic techniques. At the Stanford-US Geological Survey Micro-analytical Center (SUMAC), 39 zircon grains were handpicked under a binocular microscope and mounted on double-sided adhesive on glass slides in 1×6 mm parallel rows together with chips of the zircon standard R33 (Black et al., 2004). After being set in epoxy resin, the zircon grains were abraded to expose their central portions by using 1500 grit wet sandpaper, and then polished with 6 μm and 1 μm diamond abrasive on a lap wheel. Prior to isotopic analysis, the internal structure, inclusions, fractures and physical defects were identified with transmitted and reflected light on a petrographic microscope, and with cathodoluminescence (CL) on a JEOL JSM 5600 electron microscope (Fig. 4). Following analysis, secondary electron images were taken to locate the exact position of the spots.

U–Th–Pb analyses of zircon were conducted at the Bay SHRIMP-RG (sensitive high-resolution ion microprobe-reverse geometry) facility operated by SUMAC in a single analytical session in July 2008. Analytical procedures for zircon dating followed methods described in Williams (Williams, 1997). The primary oxygen ion beam operated at 6–7 nA and produced a spot with a diameter of ~25 μm and a depth of 1–2 μm for an analysis time of 12–13 min. Data for each spot were collected in sets of five scans through the mass range. The concentration of U was calibrated using zircon standard CZ3 (550ppm U; (Pidgeon et al., 1995)), and isotopic compositions were calibrated against R33 ($^{206}Pb^*/^{238}U = 0.06716$, equivalent to an age of 419 Ma; (Black et al., 2004)), which was analyzed every fourth scan.

Data reduction follows the methods described by Williams (1997) and Ireland and Williams (2003), and used SQUID and ISOPLOT software

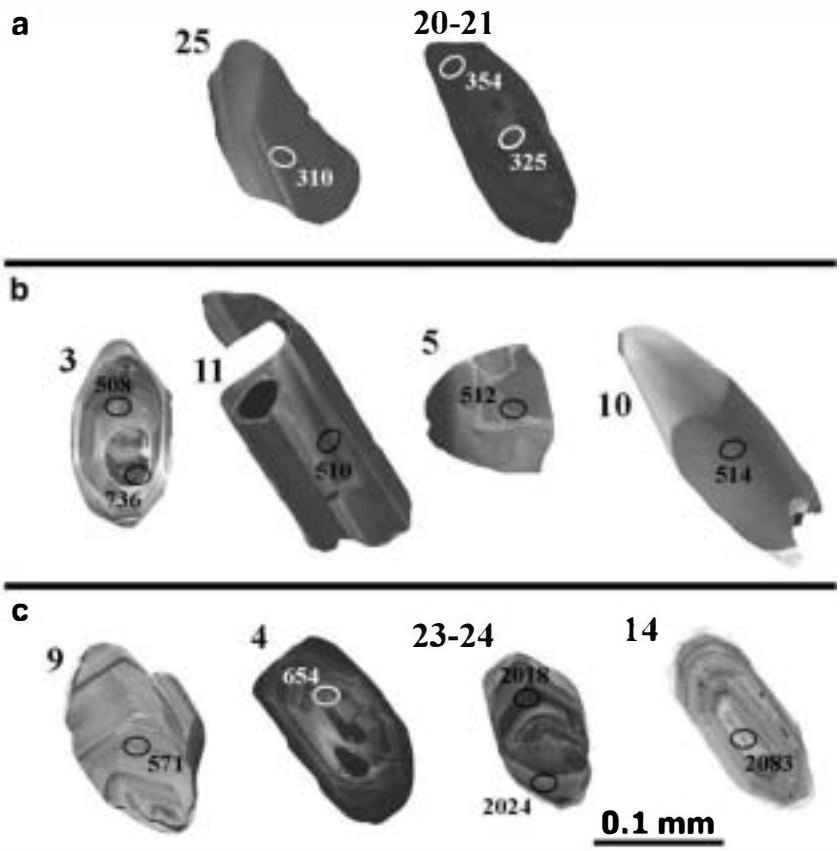

Fig. 4. Cathodoluminescence images of selected zircon crystals from the Ares dyke: (a) Variscan zircons, (b) crystallization age zircons, and (c) inherited zircons.

(Ludwig, 2002, 2003). Ages younger than 1 Ga are reported based on $^{206}Pb/^{238}U$ ratios corrected from common Pb using the ^{207}Pb method. Older ages are reported based on the ^{204}Pb-corrected $^{206}Pb/^{207}Pb$ isotopic ratio. The Pb composition used for initial Pb corrections ($^{204}Pb/^{206}Pb = 0.0554$, $^{207}Pb/^{206}Pb = 0.864$ and $^{208}Pb/^{206}Pb = 2.097$) was estimated using the Stacey and Kramers (1975) model. Analytical results are presented in Table 1 and plotted in Figs. 5 and 6.

La to Yb and Hf were measured concurrently with U–Th–Pb analysis as additional masses on each pass through the mass range. The concentrations of these elements were calibrated against an in-house standard (MAD) and are reproducible at 2–4% (1σ), except for La (15%) because of its typical very low concentration (30 ppb). U, Th, Hf and rare earth element (REE) analyses are listed in Table 2.

4.2. Zircon description and U–Pb results

The analysed zircon grains are colorless with variable length to width ratios (between 1:1 and 3:1). Most are rounded prisms with pitted surfaces, although a few are less rounded with smooth faces. Inclusions are common in all the zircon crystals. Under CL, the zircon grains show an assortment of textures suggesting for most an inherited origin (Fig. 4). Common textures include non-luminescent homogeneous zircon crystals, variably luminescent oscillatory and sector zoning, and complex grains with xenocryst cores mantled by oscillatory zoning and occasionally surrounded by an irregular non-luminescent rim.

Thirty-two analyses were obtained on 31 zircon grains (Fig. 5). The data can be roughly sorted in four age groups, <400 Ma, 480–530 Ma, 545–735 Ma and >2000 Ma (Table 1). In the first group, three scattered ages around 320 Ma could represent metamorphic ages or extreme Pb-loss from older zircon grains during the Variscan orogeny (analyses 20, 21 and 25). Since both the CL images and Th/U ratios are typically magmatic, we favour the latter interpretation. This is also in agreement with the general absence of important tectonothermal events of this age in the Órdenes Complex. From the second group, the best age estimate is obtained by pooling six analyses that yield an age of 510.53 (+8.39, −2.29)Ma using the TuffZirc algorithm (Ludwig and Mundil, 2002). This age is the median obtained from a group of 11 analyses ranging from 480 to 530 Ma, which represent the largest set of internally concordant dates that are statistically coherent, and is interpreted to date the crystallization of the Ares dyke. Ages calculated using this method are reliable provided the data are cogenetic and unaffected by Pb-loss. In this case, we argue for the validity of these assumptions based on the zircon features, namely their homogeneity and sector zoning, which are consistent with zircon growth in mafic

Table 1
SHRIMP Th–U–Pb zircon data from sample GCH-06-2 (dyke Ares-1).

Spot number and description[a]		Common ^{206}Pb (%)	U (ppm)	Th (ppm)	Th/U	$^{238}U/^{206}Pb^*$[b] (%)	$^{207}Pb/^{206}Pb^*$[b] (%)	$^{238}U/^{206}Pb^*$[c] (%)	$^{207}Pb^*/^{206}Pb^*$[c] (%)	$^{206}Pb^*/^{238}U$[d]	$^{206}Pb/^{238}U$ age[e,f]
GCH-06-2: Ares dyke											
Variscan ages											
25	m	0.12	521	813	1.61	20.27 ± 0.4	0.0535 ± 1.3	20.25 ± 0.4	0.0541 ± 1.4	0.0493 ± 0.0002	310.1 ± 1.4
21	c	0.13	833	810	1.00	19.32 ± 0.4	0.0540 ± 1.0	19.34 ± 0.4	0.0532 ± 1.2	0.0517 ± 0.0002	324.9 ± 1.2
20	r	<0.01	706	252	0.37	17.76 ± 0.4	0.0528 ± 1.2	17.77 ± 0.4	0.0524 ± 1.3	0.0564 ± 0.0002	353.5 ± 1.5
Magmatic ages											
6	m	0.14	57	48	0.87	12.90 ± 1.3	0.0579 ± 3.2	12.93 ± 1.3	0.0556 ± 3.9	0.0774 ± 0.0010	480.8 ± 6.0
31	m	<0.01	55	41	0.76	12.52 ± 1.2	0.0562 ± 3.4	12.52 ± 1.2	0.0562 ± 3.4	0.0800 ± 0.0010	496.0 ± 6.0
13	m	0.09	200	34	0.17	12.44 ± 0.6	0.0579 ± 1.6	12.46 ± 0.6	0.0567 ± 1.9	0.0803 ± 0.0005	498.1 ± 3.0
18	m	0.01	1163	638	0.57	12.35 ± 0.3	0.0574 ± 0.7	12.35 ± 0.3	0.0577 ± 0.7	0.0809 ± 0.0002	501.7 ± 1.3
22	m	<0.01	37	28	0.78	12.23 ± 1.5	0.0550 ± 3.7	12.23 ± 1.5	0.0550 ± 3.7	0.0820 ± 0.0012	**508.2 ± 7.3**
3.1	m, r	0.06	157	72	0.47	12.18 ± 0.7	0.0580 ± 2.3	12.16 ± 0.7	0.0585 ± 2.6	0.0821 ± 0.0006	**508.4 ± 3.7**
11	m	0.06	150	47	0.32	12.15 ± 0.7	0.0579 ± 1.8	12.16 ± 0.7	0.0574 ± 1.9	0.0823 ± 0.0006	**509.6 ± 3.8**
5	m	<0.01	169	108	0.66	12.11 ± 0.8	0.0574 ± 1.9	12.11 ± 0.8	0.0574 ± 1.9	0.0826 ± 0.0007	**511.5 ± 3.9**
10	m	<0.01	110	49	0.46	12.10 ± 0.8	0.0544 ± 2.1	12.11 ± 0.8	0.0537 ± 2.3	0.0825 ± 0.0007	**513.7 ± 4.3**
1	m	0.16	126	66	0.54	11.91 ± 0.8	0.0590 ± 2.0	11.92 ± 0.8	0.0584 ± 2.2	0.0838 ± 0.0007	**518.9 ± 4.0**
28	m	<0.01	151	93	0.64	11.73 ± 0.8	0.0555 ± 1.9	11.73 ± 0.8	0.0556 ± 1.9	0.0855 ± 0.0007	528.8 ± 4.0
Inherited ages											
29	m	<0.01	195	79	0.42	11.34 ± 0.6	0.0581 ± 1.5	11.35 ± 0.6	0.0571 ± 1.9	0.0882 ± 0.0006	545.1 ± 3.4
17	m	<0.01	118	70	0.61	11.14 ± 0.8	0.0585 ± 1.9	11.14 ± 0.8	0.0585 ± 1.9	0.0898 ± 0.0007	554.3 ± 4.4
27	m	0.13	104	73	0.72	10.98 ± 1.0	0.0599 ± 3.4	11.01 ± 1.0	0.0572 ± 4.2	0.0910 ± 0.0009	561.4 ± 5.5
26	m	<0.01	36	29	0.83	10.96 ± 1.7	0.0588 ± 4.1	10.99 ± 1.7	0.0563 ± 5.1	0.0913 ± 0.0016	563.0 ± 9.4
30	m	0.25	168	61	0.38	10.80 ± 0.7	0.0611 ± 1.6	10.82 ± 0.7	0.0598 ± 1.8	0.0924 ± 0.0006	569.6 ± 3.8
19	m	<0.01	264	103	0.40	10.84 ± 0.5	0.0578 ± 1.3	10.86 ± 0.5	0.0561 ± 1.8	0.0924 ± 0.0005	569.6 ± 3.0
9	m	0.22	69	37	0.55	10.78 ± 1.1	0.0609 ± 2.5	10.78 ± 1.1	0.0609 ± 2.5	0.0926 ± 0.0010	570.9 ± 5.9
32	m	<0.01	207	88	0.44	9.85 ± 0.7	0.0592 ± 1.5	9.83 ± 0.7	0.0607 ± 1.9	0.1017 ± 0.0007	624.5 ± 4.0
16	m	<0.01	302	212	0.73	9.65 ± 0.5	0.0599 ± 1.1	9.65 ± 0.5	0.0599 ± 1.1	0.1037 ± 0.0005	636.3 ± 3.0
4	m	<0.01	185	131	0.73	9.38 ± 0.6	0.0605 ± 1.4	9.37 ± 0.6	0.0612 ± 1.5	0.1067 ± 0.0007	653.8 ± 3.9
7	m	<0.01	178	73	0.43	8.38 ± 0.7	0.0634 ± 1.4	8.38 ± 0.7	0.0634 ± 1.4	0.1194 ± 0.0008	727.1 ± 4.7
3.2	c	<0.01	244	170	0.72	8.27 ± 0.5	0.0636 ± 1.1	8.28 ± 0.5	0.0633 ± 1.1	0.1209 ± 0.0007	735.7 ± 3.8
2	m	0.05	74	59	0.82	2.76 ± 0.8	0.1229 ± 0.8	2.76 ± 0.8	0.1227 ± 0.8	0.3621 ± 0.0034	1996 ± 15
23	m, r	3.14	481	174	0.37	3.50 ± 0.4	0.1244 ± 0.8	3.50 ± 0.4	0.1242 ± 0.8	0.2766 ± 0.0012	2018 ± 14
24	c	1.18	192	75	0.40	2.93 ± 0.6	0.1248 ± 1.9	2.93 ± 0.6	0.1247 ± 2.0	0.3370 ± 0.0025	2024 ± 35
12	m	<0.01	108	51	0.49	2.54 ± 0.7	0.1289 ± 0.7	2.54 ± 0.7	0.1286 ± 0.7	0.3960 ± 0.0034	2079 ± 13
14	m	<0.01	45	21	0.47	2.57 ± 1.1	0.1297 ± 1.1	2.57 ± 1.1	0.1289 ± 1.1	0.3901 ± 0.0051	2083 ± 20
15	m	0.93	142	33	0.24	1.90 ± 0.7	0.1937 ± 0.6	1.90 ± 0.7	0.1936 ± 0.6	0.5207 ± 0.0049	2773 ± 9

Bold ages represent the analyses considered to date the crystallization age of the dyke. All errors are 1σ.

[a] Zircon characterization: m = magmatic; zoned: c = core, r = rim.

[b] Uncorrected ratios.

[c] Radiogenic lead ^{204}Pb corrected for common lead.

[d] Radiogenic lead ^{207}Pb corrected for common lead.

[e] ^{207}Pb corrected for common lead.

[f] Except analyses 2, 23, 24, 12, 14 and 15 ($^{207}Pb/^{206}Pb$ age, ^{204}Pb corrected for common lead).

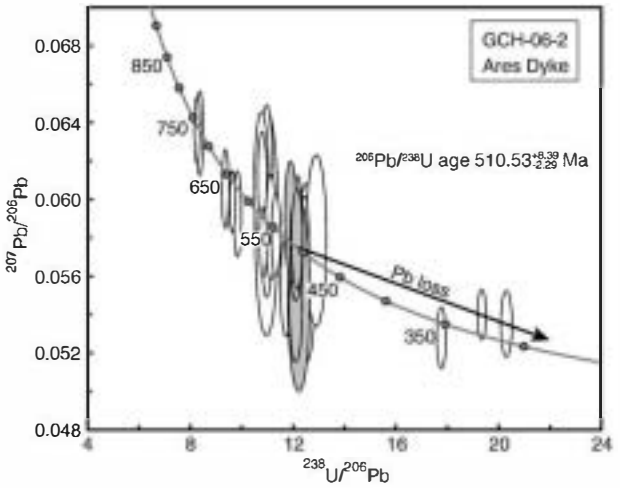

Fig. 5. Tera-Wasserburg plot showing distribution of SHRIMP zircon analyses from sample GCH-06-2. Grey ellipses correspond to analyses considered to date the crystallization age. Error ellipses are $\pm 2\sigma$.

rocks (Corfu et al., 2003). The last two age groups are interpreted as inherited components (Fig. 6) based on the variable morphology and CL features of the zircon grains. There is a cluster of six analyses at ca. 565 Ma; three single analyses between 625 and 650 Ma, and two at ca. 730 Ma. Five analyses reveal a Paleoproterozoic signature at ca. 2010 and 2080 Ma. All of these age groups match ages defined by zircon age spectra for cycles of continental crust production (Condie et al., 2009).

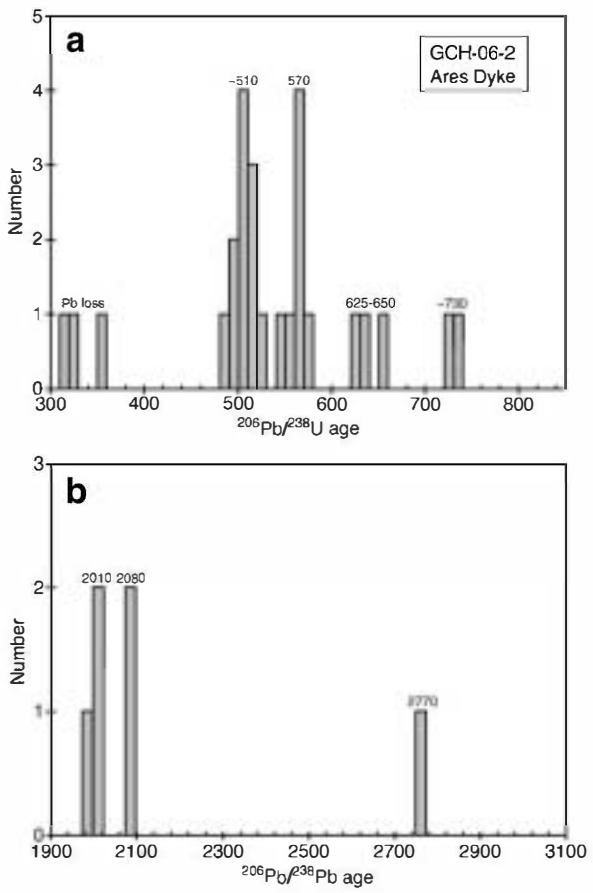

Fig. 6. Diagrams illustrating the distribution of (a) $^{206}Pb/^{238}U$ ages, and (b) $^{207}Pb/^{206}Pb$ ages from the Ares dyke zircon grains.

4.3. Trace element data

The magmatic character of the Ares dyke zircon is further supported by their rare earth element (REE) composition. Overall, their REE patterns are typical of magmatic zircon (Hoskin and Schaltegger, 2003), with low light (L) REE contents, a pronounced positive Ce anomaly, a variably negative Eu anomaly, and variable fractionation in the heavy (H) REE (Fig. 7).

Even though inter- and intra-grain compositional variation is usually large in zircons, and thus zircon REE studies should be based on both multiple zircon grains and multiple analyses per grain, some limited petrogenetic information can be suggested for the Ares dyke zircon based on their REE contents and certain elemental ratios. The following section is based on a number of general observations presented by Wooden et al. (2006) using the vast dataset obtained in their laboratory. According to these authors, Yb/Gd, which represents the steepness of the HREE pattern, appears to be an excellent monitor of magma evolution by fractional crystallization during zircon growth. For common magmatic suites, it shows a starting ratio of about 10 and increases rapidly at relatively low temperatures (<750 °C). Conversely, Th/U tends to decrease with zircon crystallization temperature, showing the strongest changes at higher temperature. The Ce/Sm ratio is preferred to that of Ce/Ce* by these authors because it varies more regularly when plotted against a fractionation index, typically showing an increase with increasing fractionation (e.g., Yb/Gd ratio).

These features are illustrated for the Ares dyke zircons in plots of Yb/Gd versus Th/U and Ce/Sm versus Yb/Gd (Fig. 8a and b, respectively). In both diagrams, the low and homogeneous Yb/Gd ratio in the zircon grains used to define the age of the dyke is apparent, consistent with crystallization from a poorly evolved magma such as a mafic dyke. Conversely, the remaining zircon grains usually show higher and more scattered Yb/Gd ratios, consistent with their inherited nature. The homogeneous character of the zircons used to determine the age of the dyke is also evident in their low Ce/Sm ratios compared to the remaining grains.

Hence, given the CL features together and characteristics of the Ares dyke zircons, it can be argued that the grains selected for the age determination represent a homogeneous population of clear magmatic rather than being of metamorphic origin. This population is clearly different from the rest of the zircon grains, which show high variability in their chemical and CL features suggesting an inherited source.

Based on the U–Pb and trace element data, a crystallization age of 510 Ma is proposed for the Ares dyke. However, the possibility that the whole zircon population is inherited cannot be completely discounted since this is a common situation in mafic rocks where the total number of zircon grains is often low. However, even if the zircon grains are inherited, this youngest zircon population would provide a maximum age of intrusion in the same way that detrital zircons provide a maximum depositional age in sedimentary rocks. In this case, the maximum age of intrusion would likely be close to the actual crystallization age. The volcanic arc preserved in the upper units of NW Iberia is characterized by an early intra-arc high-temperature metamorphism dated in the interval 505–483 Ma (Abati et al., 1999, 2007). Moreover, subsequent accretion of the arc to the southern margin of Laurussia at 410–390 Ma (Ordoñez Casado et al., 2001; Fernández Suárez et al., 2007) resulted in high-pressure/high-temperature metamorphism in the lower parts of the upper units. The absence in the dyke of a significant zircon population younger than 510 Ma, and the complete absence of metamorphic zircon grains, consequently provide additional arguments favouring its intrusion at around 510 Ma, even in the case of a completely inherited zircon population.

5. Discussion

Fuenlabrada et al. (2010) show that the sedimentary sequence in the uppermost part of the upper units has a maximum depositional age in the range 510–530 Ma (Middle Cambrian), which overlaps the

Table 2
Th, U, Hf (in ppm) and chondrite-normalized rare earth element data from zircon from sample GCH-06-2 (dyke Ares-1) and zircon standard R33.

Spot number and description		Th	U	Hf	La	Ce	Pr_{calc}	Nd	Sm	Eu	Gd	Dy	Er	Yb	Th/U	Yb/Gd	Ce/Sm	Ce/Ce*	Eu/Eu*
GCH-06-2: Sada Dyke																			
Variscan ages																			
25	m	792	485	9288	0.09	30.6	0.67	1.88	10.4	18.9	53.2	139	320	565	1.63	8.8	12.02	128	0.80
21	c	799	792	10,669	0.72	73.1	3.15	6.59	30.4	25.8	120.2	280	668	1170	1.01	8.1	9.87	48	0.43
20	r	246	662	10,703	0.05	42.1	0.54	1.67	12.4	12.0	69.9	194	561	1111	0.37	13.1	13.93	245	0.41
Ages <500 Ma																			
6	m	48	54	12,696	0.09	11.4	0.34	0.68	5.1	2.2	35.0	123	354	604	0.88	14.3	9.10	65	0.16
31	m	40	52	9877	0.08	2.6	0.79	2.46	20.7	2.2	152.2	462	1165	1781	0.77	9.7	0.50	10	0.04
13	m	34	193	11,897	0.06	1.1	0.45	1.20	17.3	1.1	184.6	1017	3200	5177	0.18	23.2	0.27	7	0.02
18	m	629	1098	11,082	0.10	83.3	1.27	4.54	42.3	10.9	343.7	1271	3338	5018	0.57	12.1	8.08	233	0.09
Dyke crystallization ages																			
22	m	27	34	7967	0.09	3.0	0.60	1.57	9.0	7.4	51.1	126	312	515	0.79	8.3	1.37	13	0.34
3.1	m, r	70	147	10,832	0.06	2.4	0.74	2.55	29.3	1.4	244.7	902	2452	3758	0.48	12.7	0.34	11	0.02
11	m	46	141	10,061	0.08	2.9	0.78	2.48	19.7	6.2	131.1	423	1139	1785	0.33	11.3	0.59	12	0.12
5	m	105	158	11,203	0.08	10.2	0.92	3.17	21.4	11.5	129.6	380	1009	1579	0.67	10.1	1.95	38	0.22
10	m	48	104	7650	0.18	3.4	1.53	4.44	34.4	25.2	225.1	636	1494	2239	0.47	8.2	0.40	6	0.29
1	m	64	118	7960	0.12	11.9	1.11	3.43	20.5	21.4	131.7	413	1177	2133	0.54	13.4	2.38	33	0.41
Inherited ages 510–600 Ma																			
28	m	91	142	10,155	0.09	7.5	1.24	4.57	34.0	6.6	211.8	578	1338	1876	0.64	7.3	0.90	22	0.08
29	m	78	184	10,287	0.18	7.3	0.56	0.98	5.1	9.1	25.4	73	237	532	0.42	17.3	5.92	23	0.80
17	m	69	111	10,793	0.07	21.9	0.39	0.89	8.1	6.2	57.4	197	572	1065	0.62	15.4	11.15	129	0.29
27	m	71	97	10,598	0.08	14.7	0.82	2.64	20.0	14.7	145.0	478	1372	2361	0.73	13.5	3.00	58	0.27
26	m	28	33	8565	0.11	10.5	0.85	2.41	13.0	16.6	61.4	152	426	830	0.84	11.2	3.33	35	0.59
30	m	60	158	10,159	7.50	11.7	2.71	1.63	3.4	4.9	16.8	59	234	654	0.38	32.3	14.07	3	0.65
19	m	101	248	11,034	0.05	22.1	0.32	0.82	7.6	3.4	55.0	198	606	1127	0.41	17.0	11.85	176	0.17
9	m	36	66	10,482	0.03	12.0	0.19	0.47	5.1	3.4	41.4	161	507	952	0.55	19.0	9.68	151	0.24
Inherited ages 600–750 Ma																			
32	m	86	193	11,218	0.11	24.5	0.34	0.58	5.8	3.3	46.6	189	689	1515	0.45	26.9	17.21	126	0.20
16	m	213	291	9917	0.21	39.9	0.89	1.82	11.3	14.1	68.7	223	692	1497	0.73	18.0	14.46	92	0.51
4	m	132	178	7737	0.09	23.6	0.48	1.10	7.5	13.1	44.9	142	426	883	0.74	16.3	12.84	114	0.71
7	m	72	167	10,657	0.05	34.9	0.22	0.47	4.5	2.8	33.6	142	461	981	0.43	24.2	31.67	340	0.23
3.2	c	169	234	10,643	0.05	30.9	0.44	1.31	11.2	8.1	76.9	275	795	1435	0.73	15.4	11.26	205	0.27
Inherited ages >2000 Ma																			
2	m	59	71	9500	0.05	28.5	0.47	1.45	9.9	5.8	58.9	170	427	688	0.83	9.7	11.75	185	0.24
23	m, r	170	448	12,322	1.51	48.6	1.17	1.02	9.2	4.7	75.2	324	1187	2469	0.38	27.2	21.59	37	0.18
24	c	74	181	12,562	0.07	46.1	0.31	0.68	6.6	4.2	53.4	222	792	1717	0.41	26.6	28.62	319	0.22
12	m	50	100	9420	0.08	26.0	0.60	1.61	10.9	7.4	60.4	181	539	1012	0.50	13.9	9.80	118	0.29
14	m	20	42	10,500	0.12	15.7	0.51	1.04	6.6	7.9	35.7	98	284	595	0.48	13.8	9.83	63	0.52
15	m	32	133	11,836	0.03	11.3	0.10	0.17	2.4	2.1	19.6	93	306	645	0.24	27.3	19.71	193	0.30
R-33 zircon standard																			
1	m	184	263	10,312	0.09	8.2	0.87	2.68	16.8	15.6	111.9	416	1384	2700	0.70	20.0	2.01	29	0.36
2	m	117	158	9174	0.13	8.3	1.19	3.64	23.9	18.6	166.0	592	1690	2863	0.74	14.3	1.43	21	0.30
3	m	137	199	10,025	0.06	7.7	0.56	1.76	13.4	13.9	95.0	345	1091	2150	0.69	18.7	2.37	43	0.39
4	m	150	180	8419	0.14	12.2	1.60	5.34	39.0	31.7	282.9	942	2459	3915	0.83	11.5	1.28	26	0.30
5	m	178	273	11,759	0.03	10.6	0.36	1.21	11.2	12.5	86.6	343	1138	2330	0.65	22.3	3.90	98	0.40
6	m	153	203	9262	0.12	9.5	1.30	4.27	26.5	19.8	178.1	675	2045	3520	0.75	16.4	1.47	24	0.29
7	m	129	194	10,484	0.05	7.4	0.69	2.69	18.1	15.4	115.5	427	1353	2565	0.67	18.4	1.68	42	0.34
8	m	95	136	9688	0.06	7.2	0.70	2.47	18.1	14.7	122.6	429	1259	2252	0.70	15.2	1.64	37	0.31
9	m	40	95	9074	0.04	4.6	0.19	0.44	4.3	4.0	36.3	153	542	1161	0.42	26.5	4.35	53	0.32
10	m	136	165	8709	0.05	16.0	0.61	2.13	16.4	13.1	126.8	500	1454	2490	0.83	16.2	4.00	20	0.29
11	m	122	158	8916	0.15	9.0	1.40	4.26	26.8	21.0	191.9	699	1974	3262	0.77	14.1	1.38	71	0.29
12	m	39	93	9252	0.03	6.0	0.25	0.75	6.9	6.1	55.8	232	785	1567	0.42	23.2	3.59	55	0.31
13	m	90	134	9895	0.04	6.7	0.41	1.37	11.9	11.3	90.2	324	989	1837	0.67	16.9	2.31	4	0.34
14	m	78	144	9264	2.37	9.4	2.80	3.05	9.6	9.5	37.4	123	412	918	0.54	20.3	3.99	41	0.50
15	m	12	35	9196	0.04	2.7	0.10	0.16	1.6	1.5	15.1	68	245	501	0.34	27.4	7.00	60	0.30
16	m	269	251	8445	0.08	13.7	0.65	1.84	14.8	12.2	112.0	435	1279	2193	1.07	16.2	3.82	53	0.30
17	m	33	75	9125	0.04	5.7	0.25	0.60	5.7	5.2	47.9	196	667	1322	0.44	22.8	4.07	92	0.32

Some elemental ratios cited in the text are also shown. Pr_N is calculated from La_N and Nd_N contents ($Pr = La_N^{1/3} * Nd_N^{2/3}$). Zircon description as in Table 1.

age range of the arc plutonic rocks of the same terrane (500–520 Ma). The turbiditic sequence of the Órdenes Complex was generated in a convergent setting, probably in an intra-arc sedimentary basin developed within a major, active volcanic arc located at the periphery of the West African Craton. This arc was likely built on the most external section of the Gondwanan margin, on thinned continental crust, and may incorporate remnants of the continental basement. The turbiditic sequence is intruded by numerous diabase dykes, one of which (near the village of Ares; Fig. 2), has now yielded a protolith age of c. 510 Ma. The structural relationships between the diabase dykes and the most important regional planar fabrics (S_1 and S_2) show these tectonic fabrics to be pre-Variscan and to have developed in the dynamic setting of the peri-Gondwanan volcanic arc. Moreover, the largely coeval development within the arc of plutonic activity,

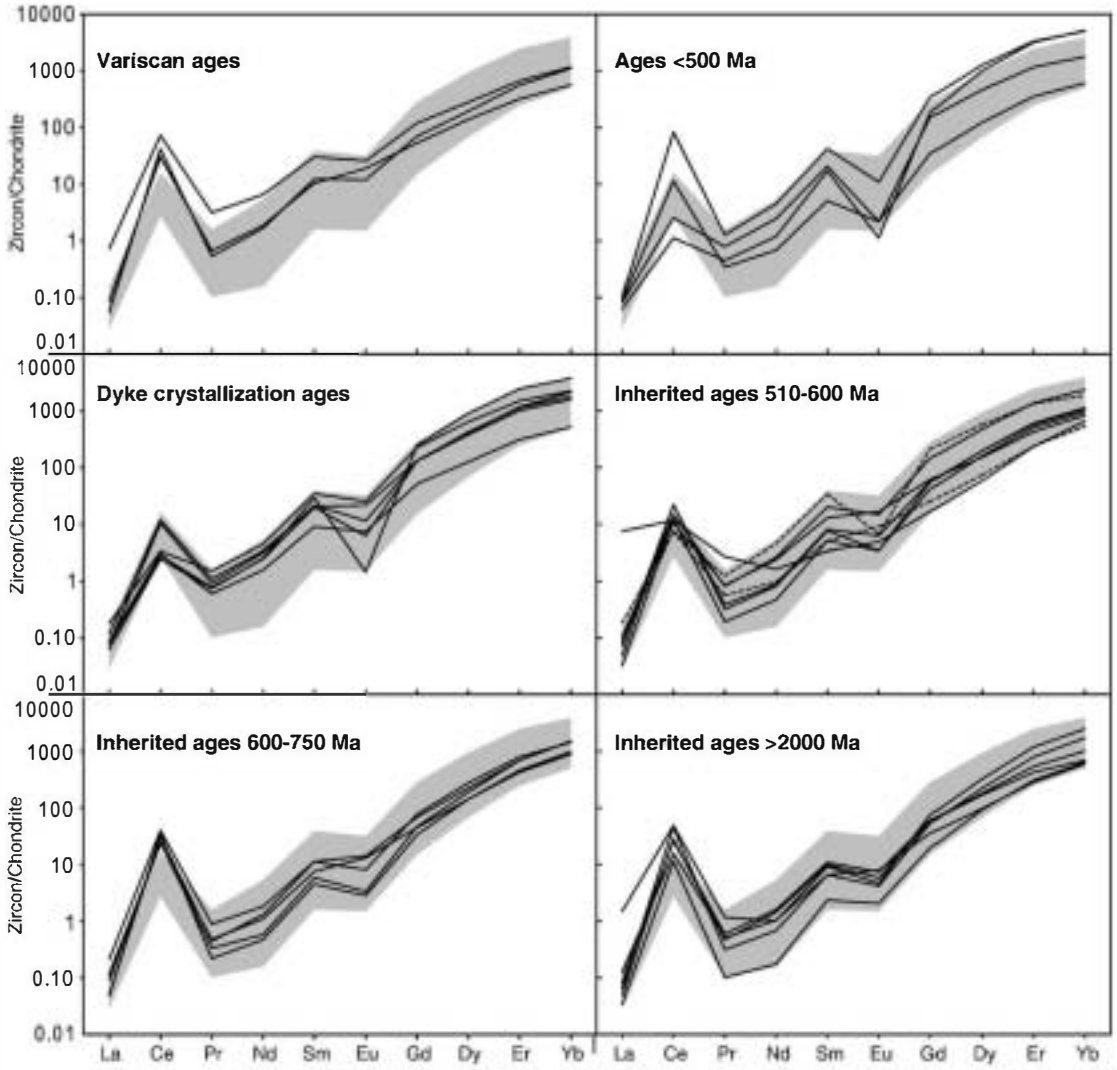

Fig. 7. Rare earth element (REE) patterns for the different age groups defined by the Ares dyke zircon crystals, illustrating their magmatic character. R33 zircon standard patterns are shown for reference (grey area), Chondrite normalization values after Anders and Grevesse (1989) modified by Korotev (1996).

deposition of turbiditic rocks in intra-arc basins, regional deformation, and the intrusion of a swarm of diabase dykes, suggest a very dynamic setting, which is typical of volcanic arcs developed on active continental margins or of island arcs.

Structural analysis of the lowest grade part of the upper unit allows the oldest dynamic history of this terrane to be examined. This study describes the structure of D_1 in the turbiditic series above the D_2 deformation front, and the link between the younger deformation to the pervasive regional

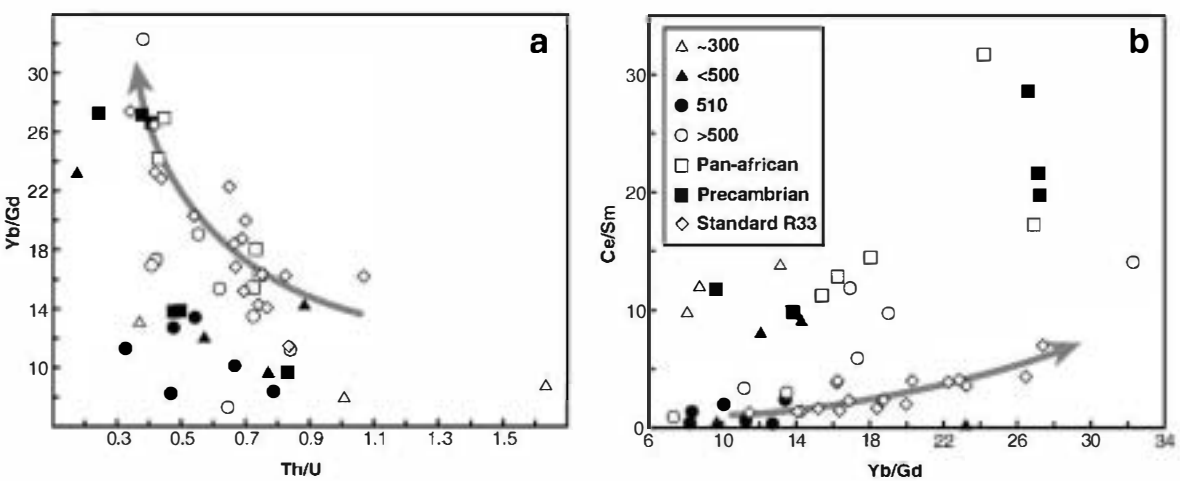

Fig. 8. Plots of (a) Yb/Gd versus Th/U, and (b) Ce/Sm versus Yb/Gd for the zircon grains analyzed in the Ares dyke. Data from R33 zircon standard (open diamonds) are included for comparison and typical magmatic fractionation trends for the standard are shown.

foliation (S_2) that affects the entire intermediate pressure upper units. In addition, the chronology of these two deformational events has been constrained by U–Pb dating of the dyke swarm and reinterpretation of previously reported detrital zircon ages (Fernández-Suárez et al., 2003). As a result, a more complete knowledge of the structural evolution of the upper units has emerged that contributes to a better understanding of the Cambrian subduction processes affecting the margin of Gondwana, and the subsequent rifting associated with the opening of the Rheic Ocean (see (Murphy et al., 2009; Santosh et al., 2009), and references therein). The vergence of the D_1 folds has remained an open question since the visionary paper of Matte and Capdevila (1978), but detailed study of the low-grade sector has revealed the existence of a fold nappe, the basic geometry of which consists of two antiform–synform pairs of west-vergent recumbent folds later folded into an upright Variscan antiform. This D_1 evolution suggests accretion below the volcanic arc, consistent with the development of a subduction zone below the external thinned margin of Gondwana, which has been previously proposed to account for the origin of the volcanic arc itself (Arenas et al., 2007; Martínez Catalán et al., 2007; Abati et al., 2009). Subduction eventually led to the accretion at the base of the arc of oceanic slices, as is suggested by evidence from the western part of the Órdenes Complex, where a thick Cambrian ophiolitic sequence (the Bazar ophiolitic unit) has been emplaced immediately below the arc-related plutonic and metasedimentary successions (Sánchez Martínez, 2009).

The development of the D_1 fold nappes was followed by a general top-to-the-north shearing event (D_2) that, in the study area, is only weakly developed and disappears upwards through a gradual deformation front. Field observations indicate that mafic dykes were emplaced at the end of the D_2 shearing. The 510 Ma protolith age obtained for the mafic dykes and the maximum depositional age obtained for the turbiditic succession (510–530 Ma), restrict the earliest stages of the tectonic evolution of the upper units to a short time interval. The regional S_2 foliation of the uppermost series can be traced downwards into the intermediate pressure upper units, where it developed under increasing temperature conditions with depth, and shows a metatexitic appearance dated at c. 490–500 Ma using U–Pb geochronology in monazites (Abati et al., 1999). This tectonic change is best interpreted in the more general framework of accretion and break up along the northern Gondwana margin. Recently, Nance et al. (2002), Murphy et al. (2006) and Linnemann et al. (2008) proposed a geodynamic model for this margin, in which latest Neoproterozoic to Early Cambrian ridge–trench collision, leads diachronously to the termination of subduction and the generation of a continental transform during the Cambrian, along which the Rheic Ocean later opened. Our data for the arc-derived upper terrane in NW Iberia indicate that accretionary processes, recorded by the D1 west-vergent fold nappes, continued until 510 Ma and that this age marks the change to a period of north-directed extension, anatexis, intrusion of arc plutonics, and emplacement of a mafic dyke swarm, eventually linked to ridge subduction. A similar family of mafic dykes with a comparable age has been described in the tectonic blocks of the Somozas mélange, the basal tectonic mélange of the allochthonous complexes of NW Iberia (Arenas et al., 2009). This mélange includes highly dismembered remnants of a volcanic arc similar to that represented in the upper units. In this case, the diabasic dykes show compositions typical of island-arc tholeiites and intrude submarine volcanic successions with calc-alkaline composition. It has been suggested that the intrusion of the tholeiitic swarm defines the transition to an extensional regime in a mature calc-alkaline arc, which would favour the development of intra-arc basins and marks the onset of the opening of the Rheic Ocean.

Acknowledgements

Financial support for this research was provided by Spanish project CGL2007-65338-CO2/BTE (Ministerio de Ciencia e Innovación). We would like to thank the SUMAC staff at Stanford University, especially Joe Wooden and Ariel Strickland, for their help in operating the SHRIMP instrument and in interpreting the results. P. Castiñeiras's stay at the SUMAC facility was financed with a "Profesores UCM en el extranjero" travel aid. The authors also thank to two anonymous referees for insightful review of the manuscript. This study is a contribution to the IGCP Project 497: "The Rheic Ocean: Origin, evolution and correlatives".

References

Abati, J., Dunning, G.R., Arenas, R., Díaz García, F., González Cuadra, P., Martínez Catalán, J.R., Andonaegui, P., 1999. EarlyOrdovician orogenic event in Galicia (NW Spain): evidences from U–Pb ages in the uppermost unit of the Órdenes Complex. Earth and Planetary Science Letters 165, 213–228.

Abati, J., Castiñeiras, P., Arenas, R., Fernández-Suárez, J., Gómez-Barreiro, J., Wooden, J., 2007. Using SHRIMP zircon dating to unravel tectonothermal events in arc environments. The early Palaeozoic arc of NW Iberia revisited. Terra Nova 19, 432–439.

Abati, J., Gerdes, A., Fernández-Suárez, J., Arenas, R., Whitehouse, M.J., Díez Fernández, R., 2009. Magmatism and early-Variscan continental subduction in the northern Gondwana margin recorded in zircons from the basal units of Galicia, NW Spain. Geological Society of America Bulletin 122 (1–2), 219–235.

Anders, E., Grevesse, N., 1989. Abundances of the elements: meteoritic and solar. Geochimica et Cosmochimica Acta 53, 197–204.

Arenas, R., Martínez Catalán, J.R., Sánchez Martínez, S., Fernández-Suárez, J., Andonaegui, P., Pearce, J.A., Corfu, F., 2007. The Vila de Cruces Ophiolite: a remnant of the Early Rheic Ocean in the Variscan suture of Galicia (Northwest Iberian Massif). Journal of Geology 115, 129–148.

Arenas, R., Sánchez Martínez, S., Castiñeiras, P., Jeffries, T.E., Díez Fernández, R., Andonaegui, P., 2009. The basal tectonic mélange of the Cabo Ortegal Complex (NW Iberian Massif): a key unit in the suture of Pangea. Journal of Iberian Geology 35, 85–125.

Berthé, D., Choukroune, P., Jeghouzo, P., 1979. Orthogneiss, mylonite and non coaxial deformation of granites: the example of the South Armorican Shear Zone. Journal of Structural Geology 1, 31–42.

Black, L.P., Kamo, S.L., Allen, C.M., Davis, D.W., Aleinikoff, J.N., Valley, J.W., Mundil, R., Campbell, I.H., Korsch, R.J., Williams, I.S., Foudoulis, C., 2004. Improved $^{206}Pb/^{238}U$ microprobe geochronology by the monitoring of a trace-element-related matrix effect, SHRIMP, ID-TIMS, ELA-ICP-MS and oxygen isotope documentation for a series of zircon standards. Chemical Geology 205, 115–140.

Castiñeiras, P., 2005. Origen y evolución tectonotermal de las unidades de O Pino y Cariño (Complejos Alóctonos de Galicia): Nova Terra, vol. 28. 279 pp.

Condie, K.C., Belousova, E., Griffin, W.L., Sircombe, K.N., 2009. Granitoid events in space and time: constraints from igneous and detrital zircon age spectra. Gondwana Research 15, 228–242.

Corfu, F., Hanchar, J.M., Hoskin, P.W.O., Kinny, P., 2003. Atlas of zircon textures. In: Hanchar, J.M., Hoskin, P.W.O. (Eds.), Zircon. Mineralogical Society of America, Washington: Reviews in Mineralogy and Geochemistry, vol. 53, pp. 468–500.

Fernández Suárez, J., Arenas, R., Abati, J., Martínez Catalán, J.R., Whitehouse, M.J., Jeffries, T.E., 2007. U–Pb chronometry of polymetamorphic high-pressure granulites: an example from the allochthonous terranes of the NW Iberian Variscan belt. In: Hatcher Jr. Jr., R.D., Carlson, M.P., McBride, J.H., Martínez Catalán, J.R. (Eds.), 4-D framework of continental crust: Geological Society of America Memoir, vol. 200, pp. 469–488.

Fernández-Suarez, J., Corfu, F., Arenas, R., Marcos, A., Martínez Catalán, J.R., Díaz García, F., Abati, J., Fernández, F.J., 2002. U–Pb evidence for a polymetamorphic evolution of the HP–HT units of the NW Iberia Massif. Contributions to Mineralogy and Petrology 143, 236–253.

Fernández-Suárez, J., Díaz García, F., Jeffries, T.E., Arenas, R., Abati, J., 2003. Constraints on the provenance of the uppermost allochthonous terrane of the NW Iberian Massif: inferences from detrital zircon U–Pb ages. Terra Nova 15, 138–144.

Fuenlabrada, J.M., Arenas, R., Sánchez Martínez, S., Díaz García, F., Castiñeiras, P., 2010. A peri-Gondwanan arc in NW Iberia. I: isotopic and geochemical constraints to the origin of the arc — the sedimentary approach. Gondwana Research 17 (2–3), 338–351.

Gomez Barreiro, J., 2007. La Unidad de Fornas: Evolución tectonometamórfica del SO del Complejo de Órdenes: Nova Terra, vol. 32. 334 pp.

Gómez Barreiro, J., Martínez Catalán, J.R., Arenas, R., Castiñeiras, P., Abati, J., Díaz García, F., Wijbrans, J.R., 2007. Tectonic evolution of the upper allochthon of the Órdenes complex (northwestern Iberian Massif): structural constraints to a polyorogenic peri-Gondwanan terrane. In: Linneman, U., Nance, R.D., Kraft, P., Zulauf, G. (Eds.), The evolution of the Rheic Ocean: from Avalonian–Cadomian active margin to Alleghenian–Variscan collision: Geological Society of America Special Paper, vol. 423, pp. 315–332.

Hoskin, P.W.O., Schaltegger, U., 2003. The composition of zircon and igneous and metamorphic petrogenesis. In: Hanchar, J.M., Hoskin, P.W.O. (Eds.), Zircon. Mineralogical Society of America, Washington: Reviews in Mineralogy and Geochemistry, vol. 53, pp. 27–62.

Ireland, T.R., Williams, I.S., 2003. Considerations in zircon geochronology by SIMS. In: Hanchar, J.M., Hoskin, P.W.O. (Eds.), Zircon. Mineralogical Society of America, Washington: Reviews in Mineralogy and Geochemistry, vol. 53, pp. 215–241.

Korotev, R.L., 1996. A self-consistent compilation of elemental concentration data for 93 geochemical reference samples. Geostandards Newsletter 20, 217–245.

Linnemann, U., Romer, R.L., 2002. The Cadomian Orogeny in Saxo-Thuringia, Germany: geochemical and Nd–Sr–Pb isotopic characterization of marginal basins with constraints to geotectonic setting and provenance. Tectonophysics 352, 33–64.

Linnemann, U., Pereira, F., Jeffries, T.E., Drost, K., Gerdes, A., 2008. The Cadomian Orogeny and the opening of the Rheic Ocean: The diacrony of geotectonic processes

constrained by LA-ICP-MS U-Pb zircon dating (Ossa-Morena and Saxo-Thuringian Zones, Iberian and Bohemian Massifs). Tectonophysics 352, 11–32.
Ludwig, K.R., 2002. SQUID 1.02, a user's manual: Berkeley Geochronology Center Special Publication, vol. 2. 17 pp.
Ludwig, K.R., 2003. ISOPLOT/Ex, version 3, a geochronological toolkit for Microsoft Excel: Berkeley Geochronology Center Special Publication, vol. 4. 71 pp.
Ludwig, K.R., Mundil, R., 2002. Extracting reliable U–Pb ages and errors from complex populations of zircons from Phanerozoic tuffs. Geochimica et Cosmochimica Acta 66, 463.
Martínez Catalán, J.R., Arenas, R., Díaz García, F., Rubio Pascual, F.J., Abati, J., Marquínez, J., 1996. Variscan exhumation of a subducted Paleozoic continental margin: the basal units of the Órdenes Complex, Galicia, NW Spain. Tectonics 15, 106–121.
Martínez Catalán, J.R., Díaz García, F., Arenas, R., Abati, J., Castiñeiras, P., González Cuadra, P., Gómez Barreiro, J., Rubio Pascual, F., 2002. Thrust and detachment systems in the Órdenes Complex (northwestern Spain): implications for the Variscan–Appalachian geodynamics. In: Martínez Catalán, J.R., Hatcher Jr. Jr., R.D., Arenas, R., Díaz García, F. (Eds.), Variscan–Appalachian dynamics: the building of the Late Paleozoic Basement: Geological Society of America Special Paper, vol. 364, pp. 163–182.
Martínez Catalán, J.R., Arenas, R., Díaz García, F., González Cuadra, P., Gómez-Barreiro, J., Abati, J., Castiñeiras, P., Fernández-Suárez, J., Sánchez Martínez, S., Andonaegui, P., González Clavijo, E., Díez Montes, A., Rubio Pascual, F.J., Valle Aguado, B., 2007. Space and time in the tectonic evolution of the northwestern Iberian Massif: implications for the Variscan belt. In: Hatcher Jr. Jr., R.D., Carlson, M.P., McBride, J.H., Martínez Catalán, J.R. (Eds.), 4-D framework of continental crust: Geological Society of America Memoir, vol. 200, pp. 403–423.
Matte, Ph., Capdevila, R., 1978. Tectonique en grands plis couchés et plissements superposés d'âge hercynien dans la série de Ordenes–Betanzos (Galice Occidentale). Cuadernos del Seminario de Estudios Cerámicos de Sargadelos 27, 193–201.
Murphy, J.B., Gutiérrez Alonso, G., Nance, R.D., Fernández-Suárez, J., Keppie, J.D., Quesada, C., Strachan, R.A., Dostal, J., 2006. Origin of the Rheic Ocean: rifting along a Neoproterozoic suture? Geology 34, 325–328.
Murphy, J.B., Nance, R.D., Cawood, P.A., 2009. Contrasting modes of supercontinent formation and the conundrum of Pangea. Gondwana Research 15, 408–420.
Nance, R.D., Murphy, J.B., Keppie, J.D., 2002. A Cordilleran model for the evolution of Avalonia. Tectonophysics 352, 11–32.
Ordoñez Casado, B., Gebauer, D., Schäfer, H.J., Gil Ibarguchi, J.I., Peucat, J.J., 2001. A single Devonian subduction event for the HP/HT metamorphism of the Cabo Ortegal complex within the Iberian Massif. Tectonophysics 332, 359–385.
Passchier, C.W., Trouw, R.A.J., 2005. Microtectonics. Springer-Verlag, Berlin. 366 pp.
Pidgeon, R.T., Furfaro, D., Kennedy, A.K., Nemchin, A.A., van Bronswjk, W., 1995. Calibration of zircon standards for the Curtin SHRIMP II. U.S. Geological Survey Circular 1107, 251.
Sánchez Martínez, S., 2009. Geoquímica y geocronología de las ofiolitas de Galicia. Nova Terra 327, 317–341.
Santosh, M., Maruyama, S., Yamamoto, S., 2009. The making and breaking of supercontinents: some speculations based on superplumes, super downwelling and the role of tectosphere. Gondwana Research 15, 324–341.
Stacey, J.S., Kramers, J.D., 1975. Approximation of terrestrial lead isotope evolution by a two-stage model. Earth and Planetary Science Letters 26, 207–221.
Williams, I.S., 1997. U–Th–Pb geochronology by ion microprobe: not just ages but histories. Economic Geology 7, 1–35.
Wooden, J.L., Mazdab, F.K., Barth, A.P., Miller, C.F., Lowery, L.E., 2006. Temperatures (Ti) and compositional characteristics of zircon: early observations using high mass resolution on the USGS-Stanford SHRIMP-RG. Third SHRIMP workshop, Rottnest Island, Australia. Program and abstracts 64–65.